Variability of rock texture and morphology correlated with the clay-bearing units at Mawrth Vallis, Mars

Nancy K. McKeown,[1] Janice L. Bishop,[2] and Eli A. Silver[3]

Received 31 May 2012; revised 26 April 2013; accepted 14 May 2013.

[1] The clay units at Mawrth Vallis have been well-characterized in hyperspectral data; however, a similar study of high spatial resolution High Resolution Imaging Science Experiment (HiRISE) data has not been previously conducted. Here the textures of the clay units are described and related to mineralogy across the central Mawrth Vallis region. The nontronite-bearing rocks appear tan in HiRISE COLOR data and are polygonally fractured with polygons 2–5 m across. In some cases, the fractures appear wider and/or have darker fill or the rocks are a darker brown. The montmorillonite-bearing rocks appear blue with regular polygons 0.5–1.5 m across; sometimes, there are larger polygons surrounded by regular polygons, a square fracture pattern, or the color appears yellow or mottled blue-yellow. Kaolinite-rich rocks are the brightest outcrops and are nonpolygonally fractured. Regions with spectra consistent with hydrated silica or the ferrous mineral component do not have unique textures. Hydrated silica-bearing rocks appear yellow or mottled with a regular polygonal texture or yellow with hummocky appearance with no polygons. It is also possible that dust/sand on the surface alters the montmorillonite spectrum to appear like that of hydrated silica. The ferrous component may be expressed as mottled coloring or as a bright fracture fill. The nontronite- and montmorillonite-bearing units have remarkably consistent textures in this region, allowing them to be uniquely identified in the Mawrth Vallis region in nonhyperspectral data sets such as CTX and HiRISE. The morphology of the polygons in these two units suggests that their formation is likely dominated by desiccation and controlled by composition.

Citation: McKeown, N. K., J. L. Bishop, and E. A. Silver (2013), Variability of rock texture and morphology correlated with the clay-bearing units at Mawrth Vallis, Mars, *J. Geophys. Res. Planets*, *118*, doi:10.1002/jgre.20096.

1. Introduction

[2] In planetary science, a major goal is to characterize the surfaces and units observed in satellite data to the greatest degree possible. Geologic maps of Mars have been created based on morphology and texture [e.g., *Scott and Tanaka*, 1986; *Greely and Guest*, 1987]; however, these were not linked directly to specific mineralogies and were created at a much larger scale than is used in this study. In the Mawrth Vallis region on Mars, extensive clay outcrops have been well-characterized in hyperspectral data, providing key mineralogical information. Here we present analyses of imaging data from the High Resolution Imaging Science Experiment (HiRISE) and compare them with mineralogy from the Compact Reconnaissance Imaging Spectrometer for Mars (CRISM) to determine if the different clay-bearing units are also distinguishable via morphology and texture.

[1]Physical Sciences, Grant MacEwan University, Edmonton, Alberta, Canada.
[2]SETI Institute, Mountain View, California, USA.
[3]Earth and Planetary Sciences, University of California Santa Cruz, Santa Cruz, California, USA.

Corresponding author: N. K. McKeown, Physical Sciences, Grant MacEwan University, Edmonton, AB, Canada. (mckeownn@macewan.ca)

©2013. American Geophysical Union. All Rights Reserved.
2169-9097/13/10.1002/jgre.20096

2. Background

[3] Mawrth Vallis is one of the oldest outflow channels on Mars, located in Noachian-aged terrains at 25°N, −20°W on the boundary between the southern highlands and northern lowlands [*Scott and Tanaka*, 1986; *Edgett and Parker*, 1997]. On the plateaus surrounding the channel are some of the most extensive clay-bearing deposits on Mars [*Noe Dobrea et al*., 2008]. Analyses of OMEGA (Observatoire pour la Minéralogie, l'Eau, les Glaces, et l'Activité on board Mars Express) data first identified nontronite and montmorillonite in the region [*Poulet et al*., 2005; *Bibring et al*., 2006; *Loizeau et al*., 2007]. CRISM (on board Mars Reconnaissance Orbiter) data analyses expanded and refined these observations, further identifying kaolinite, hydrated silica, saponite, and a ferrous mineral [*Bishop et al*., 2008a; *Wray et al*., 2008; *McKeown et al*., 2009; *Noe Dobrea et al*., 2010]. A regional, consistent stratigraphy has been identified: a nontronite-bearing unit unconformably overlain by an Al phyllosilicate unit composed of a lower layer containing montmorillonite and hydrated silica and an upper layer composed of kaolinite and hydrated silica [*Bishop et al*., 2008a; *Wray et al*., 2008; *McKeown et al*., 2009; *Loizeau et al*., 2010; *Noe Dobrea et al*., 2010; *Loizeau et al*., 2012]. A ferrous component has been identified near the boundary between the nontronite and montmorillonite

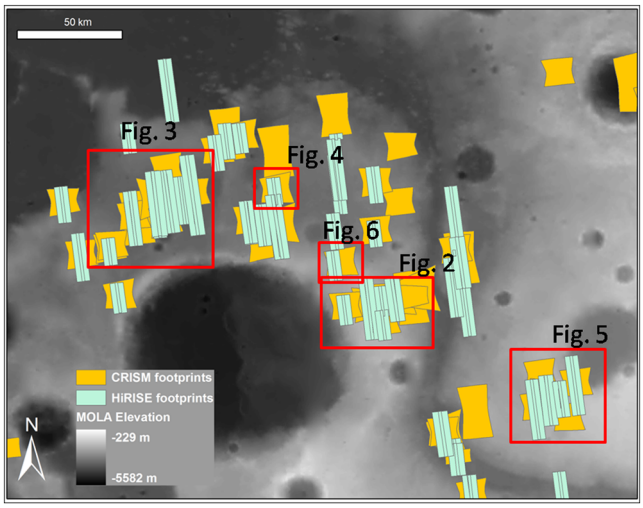


Figure 1. The central Mawrth Vallis region. CRISM image footprints are in gold, HiRISE image footprints in sea green, and the locations of five figures indicated.

units [*Bishop et al*., 2008a; *Wray et al*., 2008; *McKeown et al*., 2009; *Noe Dobrea et al*., 2010; *Bishop et al*., 2013a]. These units are capped by a spectrally unremarkable unit that is likely basaltic in composition. More recent analyses have identified potential jarosite [*Farrand et al*., 2009] and bassanite [*Wray et al*., 2010; *Noe Dobrea et al*., 2011] in isolated outcrops as well as beidellite [*Bishop et al*., 2011], allophane [*Bishop et al*., 2013b], and possibly zeolites [*Bishop et al*., 2013a].

3. Data and Methods

[4] Two CRISM image types were examined in this study: (1) full-resolution targeted images (FRTs) consist of 544 channels covering the spectral range from 0.36 to 3.92 μm at a spectral sampling of 6.5 nm, in 10–12 km wide swaths at 18 m/pixel, and (2) half-resolution long images, which have the same spectral resolution as FRTs, but have been 2× binned in the spatial dimension, giving ~36 m/pixel [*Murchie et al*., 2009]. Images were converted to *I*/*F* (the ratio of measured radiance to incoming solar flux) in preprocessing by subtracting the instrument background, dividing by processed measurements of the internal calibration standard, and dividing by solar irradiance [*Murchie et al*., 2007, 2009]. Variations in illumination geometry were corrected by dividing *I*/*F* by the cosine of the incidence angle (derived from Mars Orbiter Laser Altimeter (MOLA) gridded topography at 128 pixels/degree). Atmospheric molecular opacity effects were minimized by dividing by a scaled atmospheric transmission spectrum derived from observations over Olympus Mons [*Mustard et al*., 2008]. Images were then processed using a cleaning algorithm to remove noise and large spikes within the data due to instrument effects [*Parente*, 2008]. Band math calculations were performed to create a set of parameter maps that highlight specific spectral features [*Pelkey et al*., 2007], used to identify regions of interest for further detailed analyses.

[5] Analyzed spectra are 3×3 averages ratioed to a 3×3 average of a spectrally unremarkable region in the same column to further reduce in-column artifacts [e.g., *McKeown et al*., 2009]. In image FRT0000AA7D, spectra were retrieved from regions of interest (ROIs) averaging 50 pixels that were then

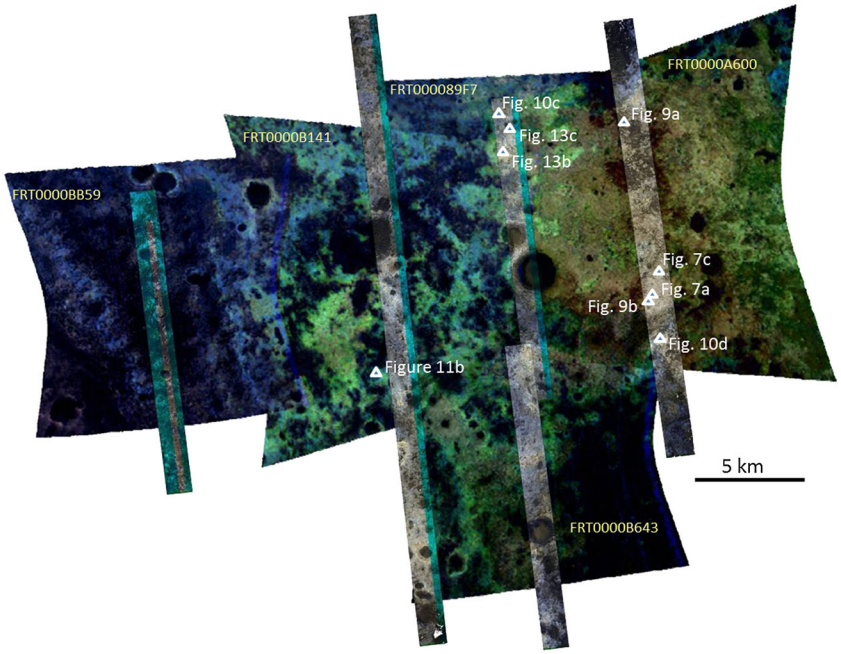


Figure 2. Locations of textures. A mosaic of CRISM images (R: 2.53 μm, G: 1.51 μm, B: 1.08 μm) overlain by mosaicked CRISM parameter maps (R: D2300, G: OLINDEX, B: BD2210) and HiRISE COLOR images. In the resulting CRISM mosaic, nontronite-bearing units appear orange/yellow, ferrous-bearing rocks appear green, and Al-phyllosilicate and hydrated silica-bearing rocks appear cyan/blue. The locations of some HiRISE textures shown in this study are indicated by white triangles. HiRISE images from left to right: PSP_009326_2040, PSP_008825_2040, PSP_005964_2045 (top), PSP_009115_2040 (bottom), and PSP_007612_2045.

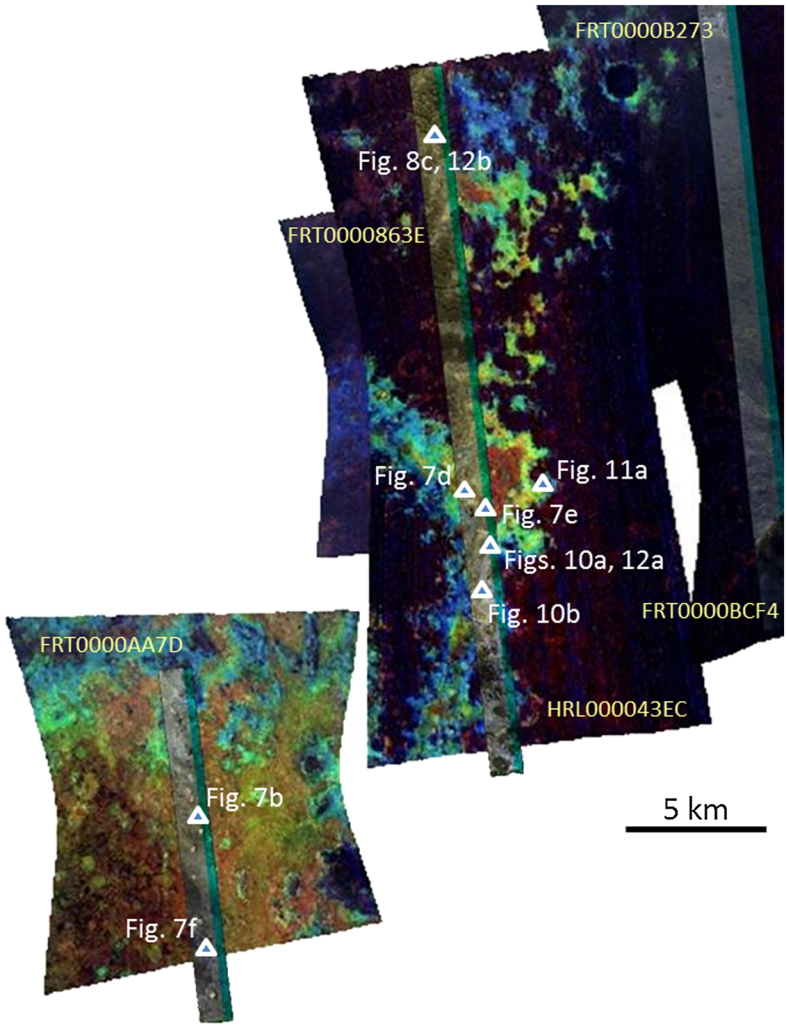


Figure 3. Locations of textures. A mosaic of CRISM images overlain by CRISM parameter maps and HiRISE COLOR images. The locations of some HiRISE textures shown in this study are indicated by white triangles. The CRISM mosaic and parameter colors are the same as in Figure 2. HiRISE images from left to right: PSP_008245_2045, PSP_006742_2050, and PSP_008891_2050.

ratioed to a spectrally unremarkable ROI. This was done due to the lack of spectrally unremarkable material in this image and the same denominator was used for all ratios.

[6] CRISM images were mosaicked using the default three bands of R: 2.53 μm, G: 1.51 μm, B: 1.08 μm and then overlain by mosaicked CRISM parameter maps using R: D2300, G: OLINDEX, B: BD2210 at 40% transparency. The D2300 parameter emphasizes the drop at 2.3 μm that occurs in Fe/Mg phyllosilicates, the OLINDEX parameter highlights regions with a positive spectral slope from 1.0–1.4 μm consistent with olivine but also with other ferrous iron-bearing minerals, and the BD2210 parameter emphasizes the band depth at 2.21 μm that occurs in Al phyllosilicates and SiOH-bearing minerals [*Pelkey et al*., 2007]. HiRISE COLOR images were then overlain on top of these to create Figures 2–6.

[7] HiRISE RED data consist of a single band covering 570–830 nm, while COLOR data consist of three bands: a blue-green (BG) channel spanning ~430–580 nm, the RED channel (same as RED data), and a near IR channel spanning ~790–1000 nm. RED data have a swath width of 6 km and COLOR data 1.2 km and both have the same spatial resolution of ~0.3 m/pixel. The HiRISE data are delivered as *I*/*F* (ratio of measured radiance to incoming solar flux), already processed for instrument artifacts, noise-reduced using a high-pass filter, and map-projected [*McEwen et al*., 2007]. Each HiRISE image was examined independent of known mineralogy and colors and textures recorded. The colors and textures were then correlated with mineralogy from CRISM data. The location of all textures shown here is indicated in Figures 1–6.

4. Results

4.1. Nontronite

[8] Nontronite-bearing units have previously been described as tan in HiRISE COLOR images with irregular polygons 2–5 m across [*Bishop et al*., 2008a; *Wray et al*., 2008; *Noe Dobrea et al*., 2010; *Loizeau et al*., 2012; *McKeown et al*., 2009] (Figure 7a) and yellow, red, and brown in High Resolution Stereo Camera (on board Mars Express) RGB images [*Loizeau et al*., 2010]. However, there are variations such as darker boundaries, darker or lighter tone, and fracture style (Figure 7).

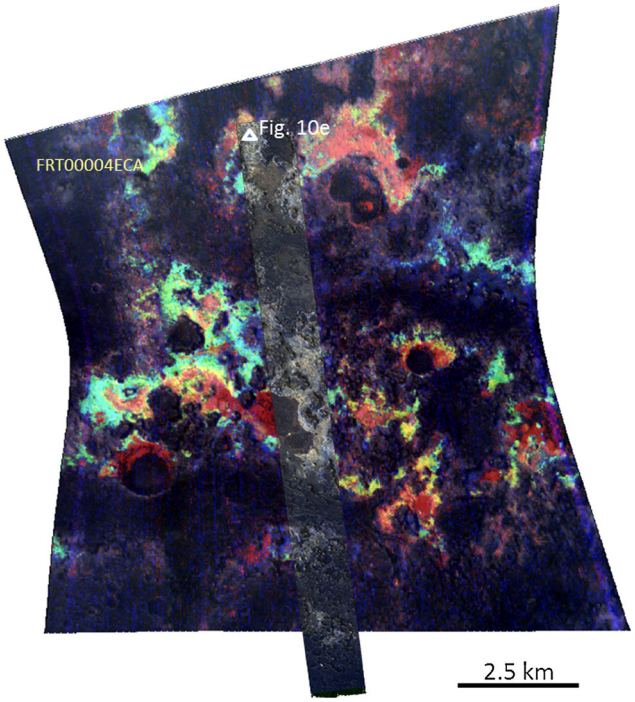


Figure 4. Locations of textures. CRISM image FRT00004ECA overlain by a CRISM parameter map and HiRISE image. The location of one HiRISE texture shown in this study is indicated by a white triangle. The CRISM mosaic and parameter colors are the same as in Figure 2. HiRISE image PSP_003036_2050.

4.1.1. Fracture Pattern

[9] In some locations, a set of almost-parallel fractures is visible in the nontronite-bearing unit (Figure 7b). In other locations, there is a radial fracture pattern (Figure 7c). These fractures radiate from a remnant butte, which could be due to an old, inverted impact crater.

4.1.2. Darker Boundaries

[10] In the standard texture of nontronite-bearing rocks (Figure 7a), the boundaries between polygons are sharp and narrow; however, in other locations, the boundaries are wider and darker (Figure 7d, 7e). It is possible that in these areas, erosion has widened the fractures between polygons, which have been filled with dark aeolian sand or dust.

4.1.3. Darker or Lighter Color

[11] While all nontronite-bearing rocks appear tan in HiRISE COLOR data, the exact shade can vary. This can sometimes be due to fracture fill (e.g., Figures 7d and 7e), but is sometimes due to other factors. Figure 7f shows an example of an underlying, darker unit that is still polygonally fractured the same way as the standard nontronite. This is possibly the Fe/Mg phyllosilicate-bearing paleosurface identified by *Loizeau et al.* [2010] or "unit 1" as identified in *Noe Dobrea et al.* [2011].

4.1.4. Bedding

[12] Bedding in nontronite is clearly visible in crater walls (Figure 8a) [*Wray et al.*, 2008] but only rarely visible on the flat plateaus (Figure 8b). Nontronite rarely forms mounds or cliffs, suggesting it may be easily eroded, which may explain why the bedding is rarely exposed except in crater walls.

4.1.5. Paleodunes

[13] In HiRISE image PSP_007612_2045 are linear features trending NW-SE and in the northern portions of the image they appear dark, rough, and linear with no abrupt changes in slope and they appear to be symmetric along the long axis (Figure 9a). Farther south in the HiRISE data, these features we interpret as paleodunes are more eroded, exposing the underlying nontronite-bearing material (Figure 9b). The paleodunes protected the underlying nontronite-bearing material, while the interdune areas continued to erode, resulting in linear "mounds" of nontronite underlying the dark paleodune material, similar to Meridiani Planum [*Sullivan et al.*, 2007], Herschel Basin, and Apollinaris Sulci [*Edgett and Malin*, 2000]. Where the paleodunes have completely eroded away, linear mounds of nontronite-bearing rocks remain that have the same polygonal texture as the surrounding, more eroded nontronite-bearing rocks (Figure 9b). These paleodunes have only been observed in this one location.

4.2. Montmorillonite

[14] Montmorillonite-bearing rocks have previously been described as blue in HiRISE COLOR images with regular polygons 0.5–1.5 m across [*Bishop et al.*, 2008a; *Wray et al.*, 2008; *Loizeau et al.*, 2012; *McKeown et al.*, 2009] (Figure 10a) and blue-white in HRSC RGB images [*Loizeau et al.*, 2010]. Variations are observed in polygon size and shape, color, and surface cover.

4.2.1. Polygon Size and Shape

[15] Generally, the polygons in montmorillonite-bearing rocks are very consistent in size and shape. In some cases, however, there are larger irregular polygons within the more standard texture (Figure 10b). In others, a square, grid-like pattern is observed (Figure 10c).

4.2.2. Color

[16] Frequently, the montmorillonite-type polygonal texture is observed with a yellow/light tan color rather than blue (Figure 10d) or with a mottled blue/yellow color (Figure 10e). It appears, however, that the mottled areas have a hillocky morphology, so it is possible the color differences also correlate to changes in elevation. The yellow-colored montmorillonite rocks are also associated with regions where material from the capping unit has eroded and been deposited downhill onto the montmorillonite-bearing rocks, making their spectrum more "red" and therefore making those areas appear yellow in the HiRISE stretch. These color differences also tend to occur close to the boundary with the nontronite and could indicate the presence of the ferrous component or hydrated silica (discussed below).

4.2.3. Bedding

[17] Bedding within the montmorillonite-bearing unit is visible both in crater walls (Figure 8a) and on the plateaus (Figure 8c), although it is often not as clear as in the nontronite-bearing unit. The bedding appears to be on the meter scale with no cross-bedding; however, HiRISE has a spatial resolution of 0.3 m/pixel so any bedding or cross-bedding narrow than ~0.6 m will not be detectable on crater walls but might be detectable in regions of shallow gradients on the plains.

4.3. Kaolinite

[18] Kaolinite-bearing outcrops appear the brightest of all clay-rich outcrops in the Mawrth Vallis region (Figure 11).

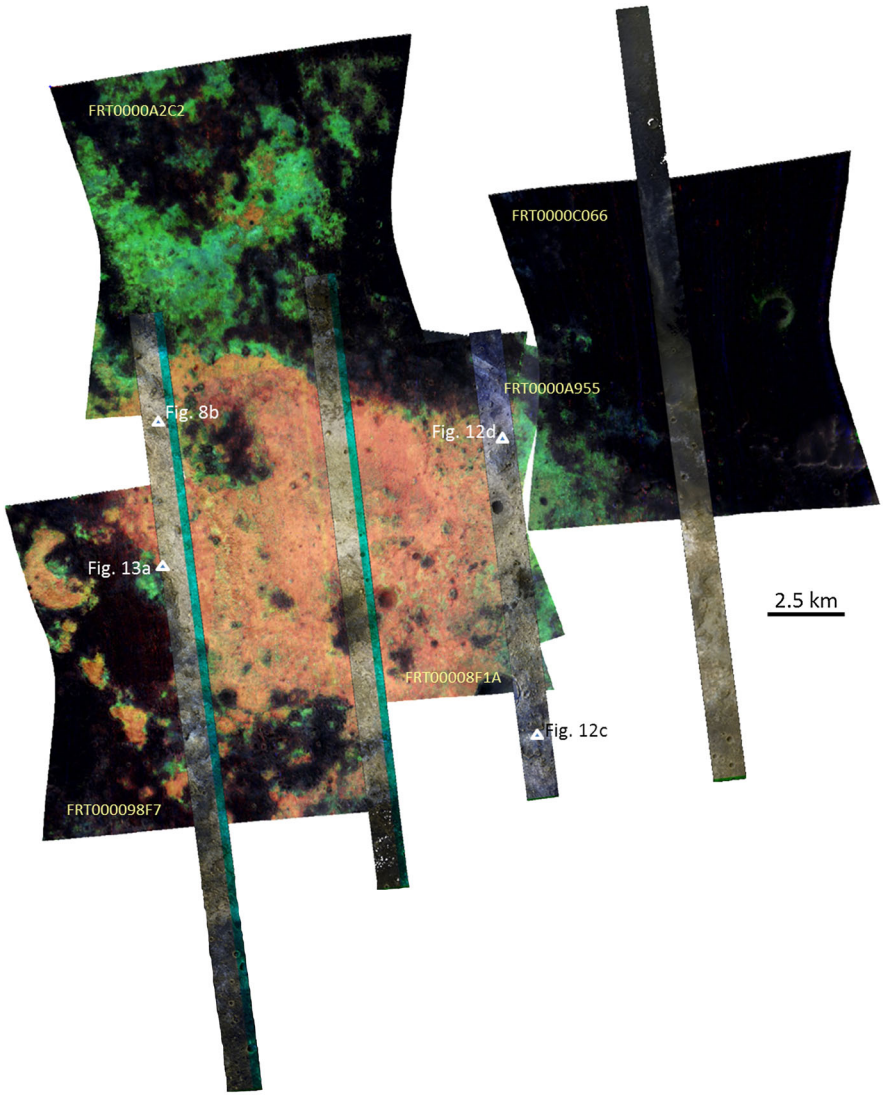


Figure 5. Locations of textures. A mosaic of CRISM images overlain by CRISM parameter maps and HiRISE COLOR images. The locations of some HiRISE textures shown in this study are indicated by white triangles. The CRISM mosaic and parameter colors are the same as in Figure 2. HiRISE images from left to right: PSP_006966_2035, PSP_006610_2035, PSP_010183_2035, and PSP_009616_2035.

They are fractured but nonpolygonally. These fractures are generally only observable in HiRISE images after stretching to enhance variation in higher-albedo areas only. The examples shown here are from HiRISE RED images because there is not yet any COLOR coverage of known kaolinite outcrops. In several locations in HiRISE images, brighter outcrops are observed that could be kaolinite; however, they are generally too small to be detected by CRISM.

4.4. Hydrated Silica

[19] Several different textures, morphologies, and colors are observed in regions dominated by hydrated silica: (1) sand/dust on the surface (Figures 12a and 12b), (2) a yellow or mottled coloring (Figures 12b–12d), or (3) the "smooth" and "fluffy" texture of mantled hummocks (Figure 12d) previously described by *Bishop et al*. [2008a]. Spectral analyses indicate that the hydrated silica is likely present in an intimate mixture with montmorillonite [*McKeown et al*., 2011], meaning they are mixed at the outcrop scale, which may be why no single texture or color is associated with hydrated silica.

4.4.1. Sand/Dust on the Surface

[20] Experiments by *Bishop* [1996] found that for spectra of ferrihydrite-montmorillonite mixtures, the ferrihydrite dominated in the visible-near infrared and in spectra of hematite-montmorillonite mixtures, the montmorillonite band depth was greatly reduced in the short-wave infrared. Thus, if the dust/sand contains a ferric oxide component, it could be altering the spectrum to resemble that of hydrated silica when in fact it is a montmorillonite-bearing rock covered by this dust/sand. Sometimes the aeolian component appears the same blue color in HiRISE as the montmorillonite-bearing rock (Figure 12a, diagonal lighter-toned material), but other times it appears darker (Figure 12b, yellow-brown material primarily on the flanks of the mound).

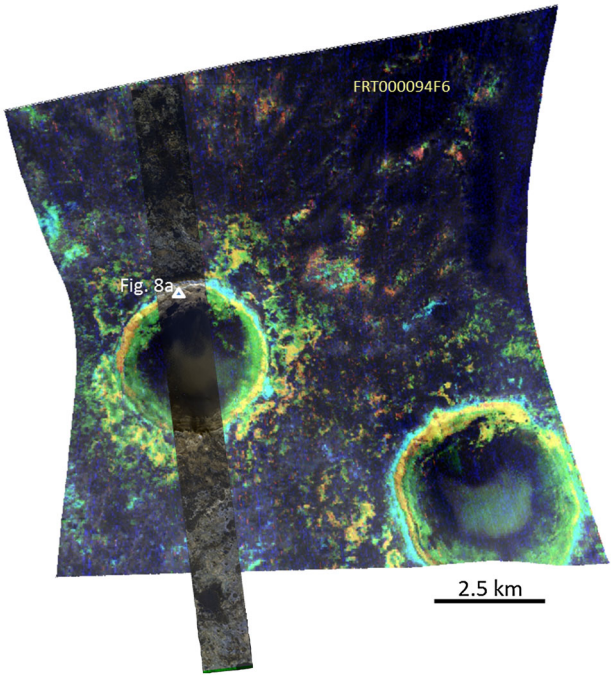


Figure 6. Locations of textures. CRISM image FRT000094F6 overlain by a CRISM parameter map and HiRISE COLOR image. The location of one HiRISE texture shown in this study is indicated by a white triangle. The CRISM mosaic and parameter colors are the same as in Figure 2. HiRISE image PSP_004052_2045.

4.4.2. Yellow or Mottled Coloring

[21] As mentioned above in the montmorillonite description, there are regions in the Al phyllosilicate unit that appear yellow (Figures 12b and 12d) or mottled yellow-blue (Figure 12c) that correspond to areas with spectra more consistent with hydrated silica rather than pure montmorillonite. In some cases, the mottled coloring is paired with a smooth, nonpolygonal texture (Figure 12c), suggesting there is not as much montmorillonite present, whose desiccation may be one source of the polygonal fractures [*Plummer and Gostin*, 1981, and references therein]. However, the mottling is sometimes also associated with the ferrous component (discussed below).

4.4.3. Smooth, Fluffy Texture

[22] Some hydrated silica-bearing rocks have a fluffy, feathery texture as first reported in *Bishop et al*. [2008a] consistent with mantled hummocks. Closer inspection reveals this texture may be due to enough sand/dust on the surface to form bright dunes or ripples and smooth over topography (Figure 12d). There are no montmorillonite-type polygons visible, possibly due to the sand/dust on the surface which also affects the spectrum making it more similar to hydrated silica than to montmorillonite as discussed above.

4.5. Ferrous Component

[23] The ferrous component has been identified in both nontronite- and montmorillonite-bearing rocks near the boundary between these two mineralogies [e.g., *Bishop et al*., 2008a; *McKeown et al*., 2009]. Like the hydrated silica-bearing outcrops, there are several different textures, morphologies, and colors associated with ferrous iron-bearing rocks. In some locations, the ferrous component is detected in areas with the bright fractures that occur near the nontronite/montmorillonite unit boundary (Figures 13a and 13b). However, these bright fractures tend to only occur with small-to-intermediate sized polygons (~0.9–2.1 m across) and not in the larger nontronite-like polygons. Also, these bright fractures are sometimes observed away from the unit boundary in the midst of montmorillonite-bearing outcrops (Figure 13c). Thus, if these bright fractures contain the ferrous component, it may have formed through fluid circulation that acted at varying elevations throughout the montmorillonite-bearing unit. Another possibility is that the ferrous component is expressed as a mottled yellow/blue coloring (Figures 10e, 12c, and 13b) because this coloring only occurs at the boundary between the nontronite- and montmorillonite-bearing units. However, this ferrous component has also been identified mixed with nontronite, which does not exhibit any mottling.

4.6. Spectral Results

[24] Spectra of nontronite have hydration absorptions at 1.42 and 1.91 μm, an Fe-OH absorption at 2.29 μm, and another absorption at 2.41 μm. Spectra of montmorillonite have hydration absorptions at 1.41 and 1.91 μm and a sharp

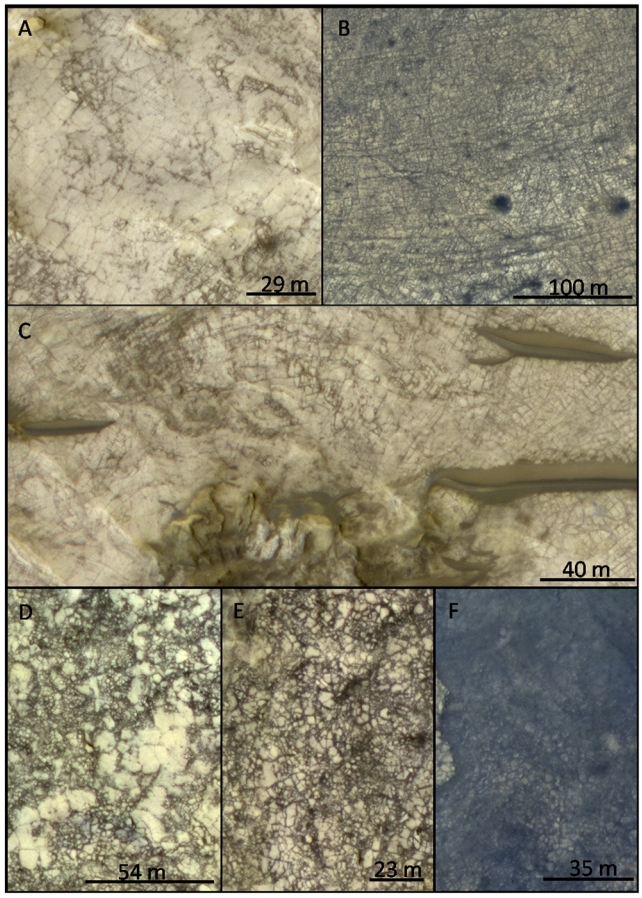


Figure 7. Examples of textures of nontronite-rich rocks. (A) "standard" nontronite-rich outcrop, (B) extensive parallel fracture set, (C) radial fracture set, (D and E) nontronite-rich outcrop with dark, thicker fracture fill, and (F) darker, lower nontronite-bearing material.

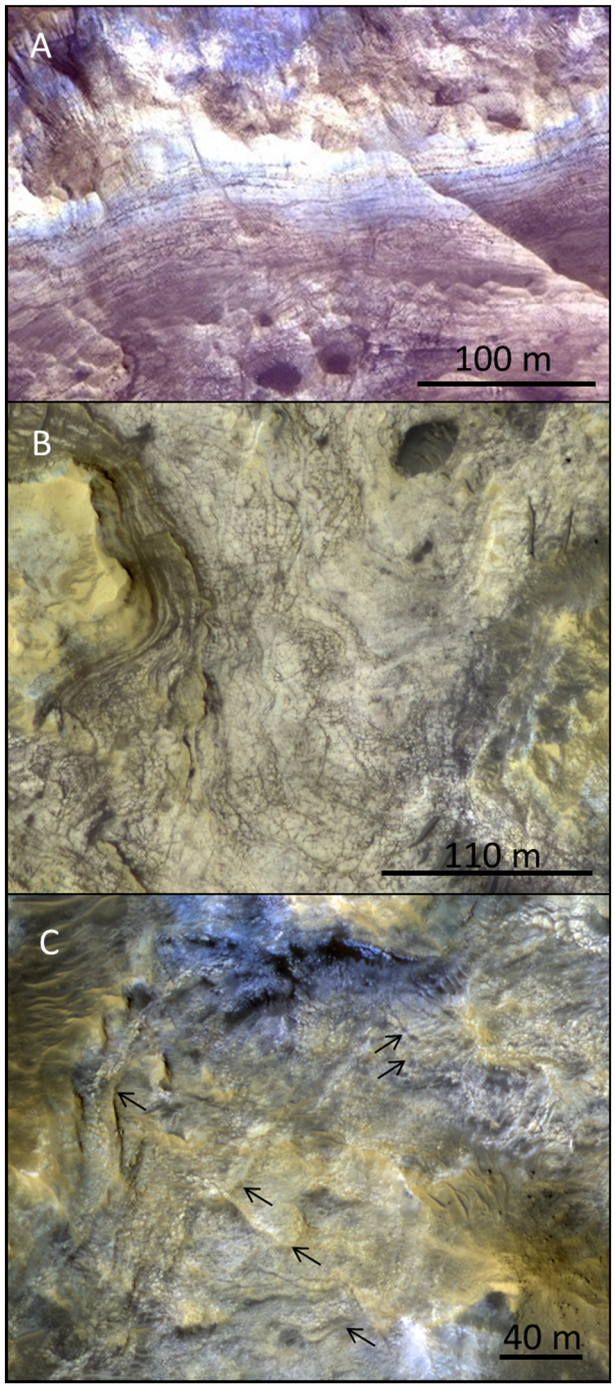


Figure 8. Examples of bedding: (A) Bedding exposed in a crater wall in both nontronite- (lower, tan) and montmorillonite-bearing (upper, blue) units (for a detailed description of these units, see *Wray et al*. [2008]; (B) bedding in nontronite exposed on the plateaus; and (C) bedding in montmorillonite exposed on the plateaus, some of which are indicated with black arrows. In general, bedding is clearer in the nontronite-bearing unit than the montmorillonite-bearing unit.

Al-OH absorption at 2.21 μm. Spectra of hydrated silica have a weak 1.93 μm absorption and a broad 2.2 μm Si-OH absorption [*Anderson and Wickersheim*, 1964; *Bishop et al*., 2004; *Milliken et al*., 2008]. Spectra of kaolin family minerals are characterized by a doublet absorption at ~1.39 and 1.41 μm due to OH stretch overtones and a second doublet feature at ~2.17 and 2.21 μm due to Al-OH stretching and bending [e.g., *Bishop et al*., 2008b]. Some spectra observed in Mawrth Vallis have a strong positive slope from 1.0 to 2.0 μm, possibly due to a ferrous component. Fe^{2+} in octahedral sites has overlapping absorption bands at 1.02, 1.04, and 1.05 μm and Fe^{2+} in tetrahedral sites in pyroxenes has an absorption in the range 1.80 to 2.30 μm [*Burns*, 1993]. The focus of this paper is not the mineralogic identification of spectra in the Mawrth Vallis region; this has been extensively covered by many studies [*Bibring et al*., 2005; *Poulet et al*., 2005; *Bibring et al*., 2007; *Loizeau et al*., 2007; *Bishop et al*., 2008b; *Poulet et al*., 2008; *Wray et al*., 2008; *Farrand et al*., 2009; *McKeown et al*., 2009; *Loizeau et al*., 2010; *Noe Dobrea et al*., 2010; *Wray et al*., 2010; *Noe Dobrea et al*., 2011]. However, a major goal of the study is to correlate the mineralogy with the textures of the main

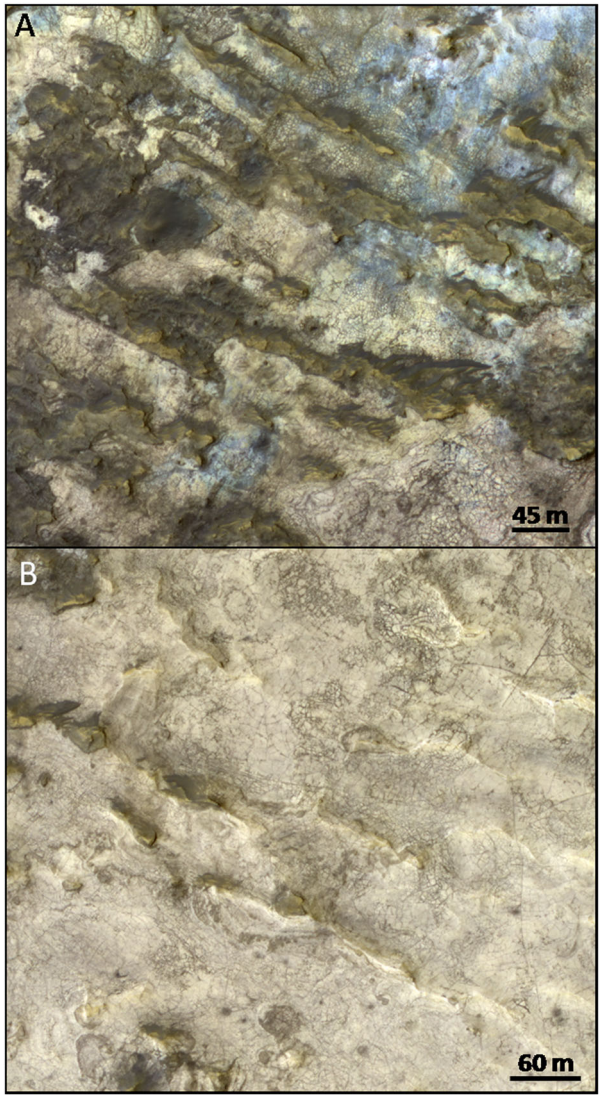


Figure 9. Examples of paleodunes: (A) Paleodunes (dark brown) in HiRISE COLOR PSP_007612_2045 trending NW-SE across the image, superposed on the nontronite (tan) and montmorillonite (blue) units. (B) Mounds of nontronite-rich rock that remain after the dark paleodune material has been eroded away from farther south in the same HiRISE image.

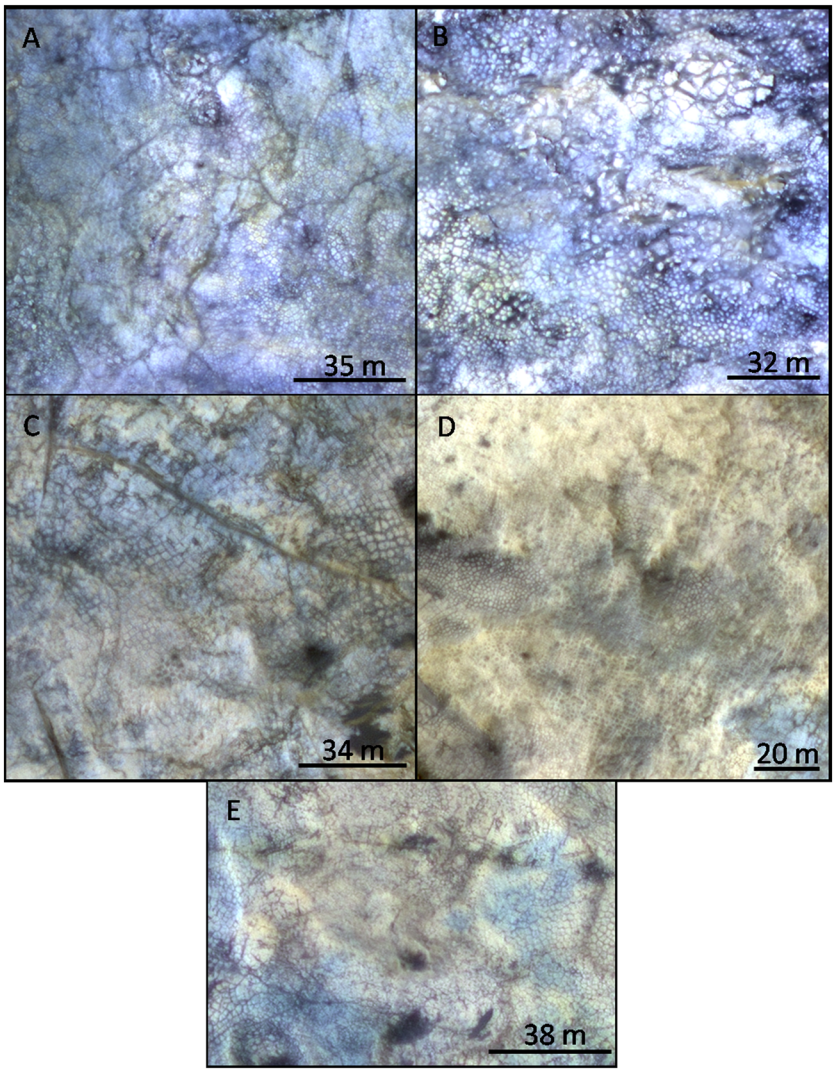


Figure 10. Examples of textures of montmorillonite-rich rocks. (A) "Standard" montmorillonite-rich outcrop with regular polygons 0.5–1.5 m across, (B) larger polygons surrounded by the standard montmorillonite-rich texture, (C) square polygonal pattern, (D) standard texture but yellow rather than blue coloring, and (E) standard texture with mottled yellow/blue coloring.

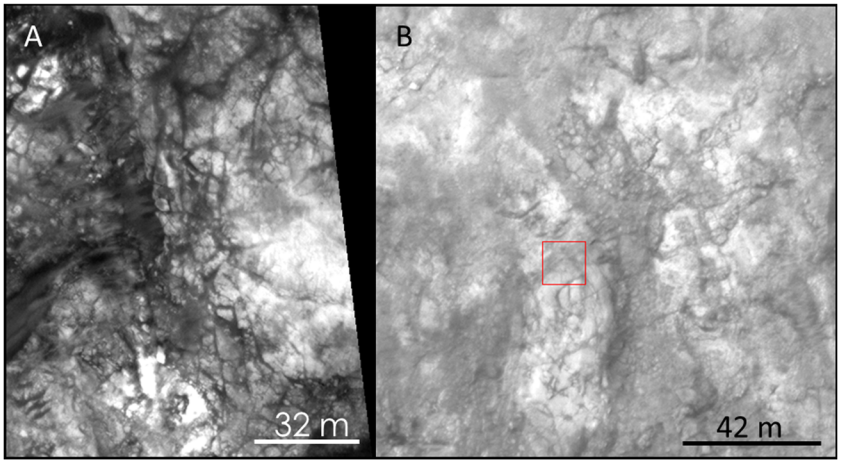


Figure 11. Two examples of the very bright, fractured kaolinite-bearing material.

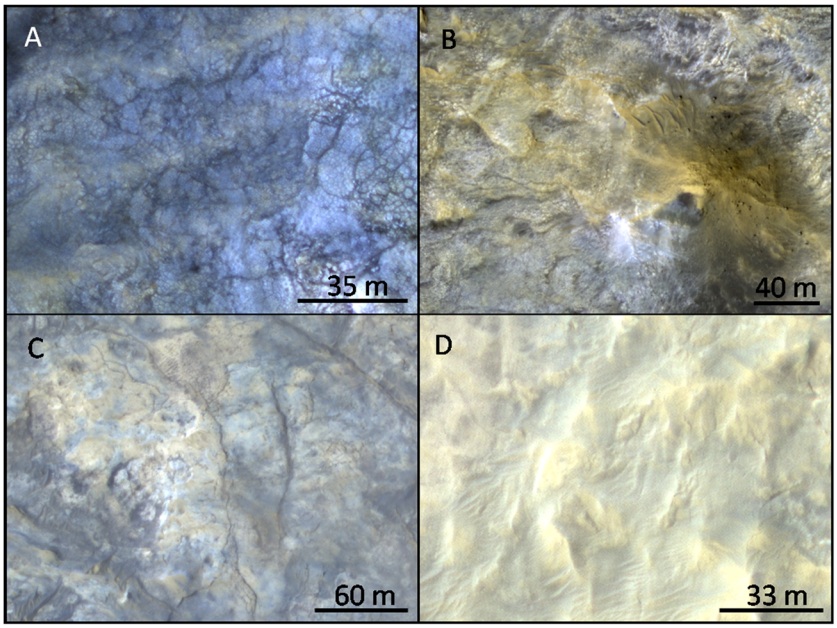


Figure 12. Possible textures of hydrated silica-bearing rocks. (A) Aeolian material (yellow/light colored streaks trending ENE-WSW) on top of montmorillonite-bearing rock; (B) dark aeolian material on montmorillonite-bearing rock and yellow color; (C) mottled coloring, smooth texture; and (D) smooth, fluffy texture with yellow coloring.

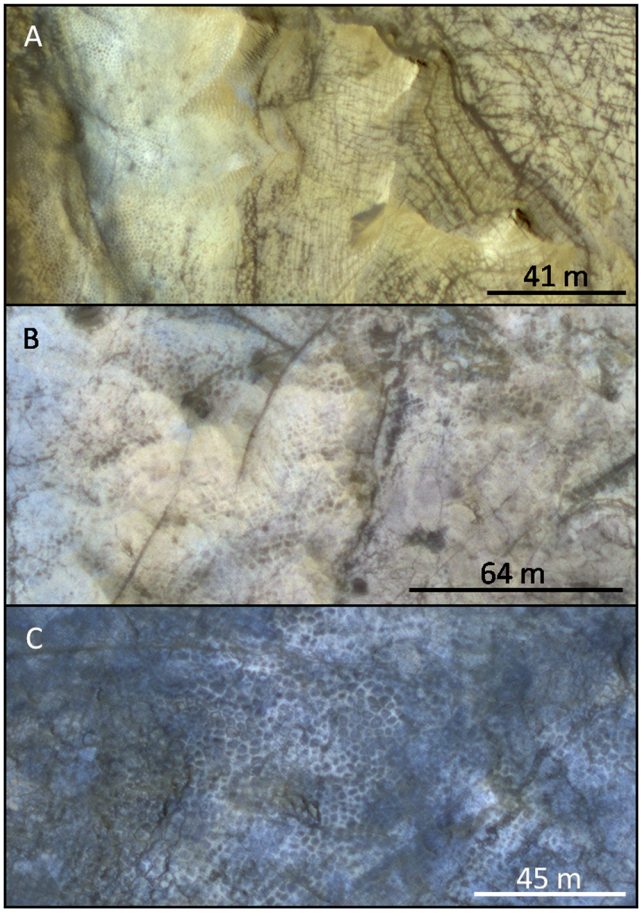


Figure 13. Examples of bright fractures that may be the ferrous component. (A) Around montmorillonite-type polygons (left side of image) at the boundary between the nontronite- and montmorillonite-bearing units, (B) within mottled coloring, and (C) within the montmorillonite-bearing unit.

clay-bearing units. Therefore, spectra were retrieved from each of the locations discussed in the previous sections and are displayed in Figure 14. A spectrum for Figure 8a is not included because of the multiple mineralogies displayed and the extensive area covered (we refer the reader to *Wray et al*. [2008] for mineralogic analysis of this region) nor for Figure 12d because there is no CRISM image associated with that location.

5. Discussion

[25] Comparing mineralogy and morphology/texture, the nontronite-bearing unit shows remarkable consistency in texture and color. Any changes in morphology, such as the paleodune casts, retain the irregular polygonal fracture texture making it easy to identify. The montmorillonite-bearing unit, on the other hand, has a greater variety of textures; although, they all exhibit either small, regular polygonal fractures or blue coloring. It is possible the montmorillonite-bearing rocks exhibit a greater variety of textures because the rock contains hydrated silica and other mineral components in varying amounts whereas the nontronite-bearing rocks appear to be more uniform in composition in spectral data. The textures of rocks containing hydrated silica or ferrous mineral may be more difficult to identify because they are not major mineral components or have a weaker influence on the texture than the nontronite and montmorillonite.

5.1. Color Differences

[26] One of the most striking differences between the nontronite- and montmorillonite-bearing units is the color: montmorillonite typically appears blue in color, whereas nontronite appears tan. The blue color of montmorillonite in HiRISE data is due primarily to having a spectral slope in visible wavelengths that is less "red" than the nontronite spectra [*Loizeau et al*., 2010], making it appear blue in the

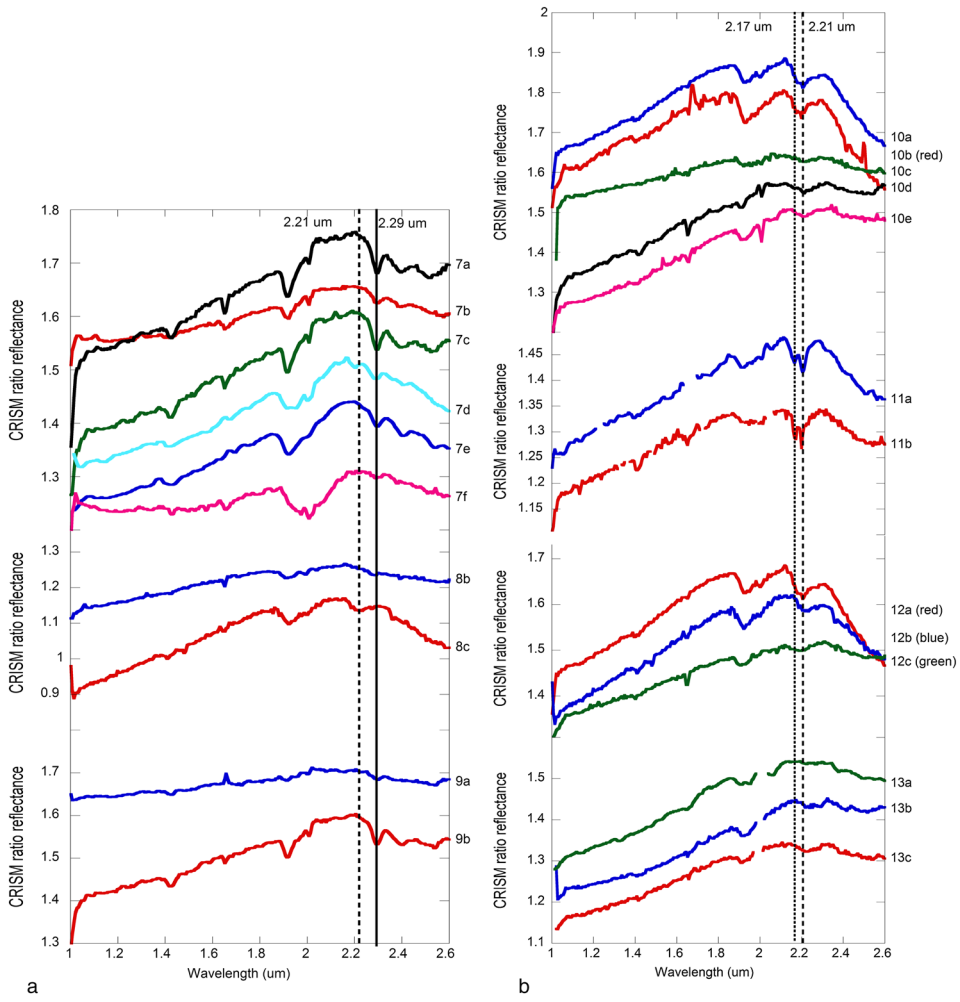


Figure 14. Spectra from the HiRISE locations shown in Figures 7–13; the figure number is indicated to the right of the spectrum. Vertical lines indicate the key absorption features that were used to distinguish between nontronite, montmorillonite, hydrated silica, and kaolinite. Gaps in the spectra are due to removal of noise and spectra are offset for clarity. (A) Spectra for Figures 7–9: mainly nontronite spectra with the exception of spectrum 8c. (B) Spectra for Figures 10–13: Al phyllosilicate or hydrated silica spectra.

default HiRISE image stretch [*Delamere et al*., 2010]. This is not common in laboratory montmorillonite spectra, but is consistent with bedrock in HiRISE data [*Delamere et al*., 2010].

5.2. Polygon Formation

[27] The other striking difference between the nontronite- and montmorillonite-bearing units is the morphology of the polygons. The polygonal pattern observed in the nontronite- and montmorillonite-bearing rocks is similar to that due to wet-dry cycles, such as mud-cracks [e.g. *Plummer and Gostin*, 1981, and references therein] or that of thermal contraction (e.g., freeze-thaw) cycles such as that found in permafrost environments both on Earth [e.g., *Lachenbruch*, 1962] and Mars [e.g., *Mellon et al*., 2008]. However, the polygons at Mawrth Vallis are mostly smaller than those identified by *Levy et al*. [2009] as being of thermal contraction origin and as Mawrth Vallis is located near the boundary (25°N) where thermal contraction polygons can easily form (20°–30° latitude) [*Mellon*, 1997], it may be more difficult for them to form here than at other latitudes, suggesting thermal contraction may not be the primary formational mechanism. None of the fractures observed at Mawrth Vallis are consistent at the observed scale with subaerial Sun-cracks that occur when loose aeolian sediment is moistened and contracts [*Swartz*, 1927]. In cases where other factors such as impacts are likely influencing fracture formation (e.g., Figure 7c), the pattern due to the impact almost always overprints the "standard" nontronite texture rather than replaces it.

[28] Therefore, desiccation is probably the primary mechanism controlling the formation of these polygons. Factors that influence the formation of desiccation cracks (mud-cracks) include composition, salinity of the water, temperature, persistence of wet-dry cycling, and bed thickness; in general, larger polygons form with greater bed thickness, homogeneity, salinity, and/or temperature [e.g., *Plummer and Gostin*, 1981 and references therein]. Multiple generations of cracks can form in highly expansive clays [*Kindle and Cole*, 1938] such as montmorillonite. Therefore, based on polygon morphology, the beds within the nontronite-bearing unit may be thicker and the composition more homogenous than that of the montmorillonite unit; the latter is supported by the compositional

evidence from CRISM and OMEGA data analyses [*Loizeau et al*., 2007; *Bishop et al*., 2008a; *Wray et al*., 2008; *McKeown et al*., 2009; *Noe Dobrea et al*., 2010]. It is likely that composition is one of the primary factors controlling the morphology of the polygons in the Mawrth Vallis region, with the more homogenous nontronite-bearing unit resulting in larger polygons and the less homogenous and more expansive montmorillonite-bearing unit resulting in smaller polygons. As an addendum, similar polygons have been observed in Fe/Mg-phyllosilicate-bearing rocks near the Valles Marineris [e.g., *Le Deit et al*., 2010, 2012] and in Noachis Terra [*Buczkowski and Seelos*, 2010], suggesting that phyllosilicate composition may be a strong determinant of texture for rocks of this composition in latitudes $<30°$.

6. Conclusion

[29] Textures for nontronite-bearing rocks (tan, irregular polygons 2–5 m across) and montmorillonite-bearing rocks (blue and/or yellow, regular polygons 0.5–1.5 m across) are distinctive and easily identified in HiRISE data, even with variations. The few textural examples of kaolinite-bearing outcrops are very bright in comparison and fractured. Neither hydrated silica nor the ferrous mineral component have a clearly identifiable texture. It is possible that rocks containing hydrated silica have a smooth texture and a mottled appearance; however, there is also a possibility that the spectrum similar to hydrated silica is due to sand/dust on top of the montmorillonite-bearing rock. The ferrous mineral component is possibly expressed as a bright fracture fill between polygons or as a mottled coloring. The bright fracture fill does not occur exclusively at the boundary between the nontronite- and montmorillonite-bearing units, which makes it a less likely candidate. The mottled coloring is only associated with the montmorillonite texture, so it too is only a possibility because the ferrous component is not only mixed with the montmorillonite-bearing rock but also with the nontronite-bearing rock near the boundary between the two units.

[30] The textures of nontronite- and montmorillonite-bearing rocks are consistent throughout the entire central Mawrth Vallis region: the first time mineralogic units have been correlated with specific, unique textures across a large area, not just in specific images. This consistency permits the identification of the nontronite-bearing unit and montmorillonite-bearing units in panchromatic data such as CTX or HiRISE RED images and three-band data such as HiRISE COLOR images. The morphology of the polygons suggests that their formation is likely dominated by desiccation and controlled by composition. These correlations between mineralogy and texture only apply to the Mawrth Vallis region, however, and cannot be applied to other regions of Mars unless the unit in question has a similar mineralogy and experienced a similar postdepositional environment. That being said, observations of nontronite-bearing rocks near Valles Marineris, Noachis Terra, and elsewhere on Mars exhibit a very similar color and texture, suggesting that composition is the dominant factor controlling the appearance of these units.

[31] **Acknowledgments.** We would like to thank Francis Nimmo, Erik Asphaug, Damien Loizeau, and an anonymous reviewer for their helpful comments, which greatly improved this manuscript, and NASA's Mars Data Analysis Program for support of this research.

References

Anderson, J. H., and K. A. Wickersheim (1964), Near infrared characterization of water and hydroxyl groups on silica surfaces, *Surf. Sci.*, *2*, 252–260.

Bibring, J.-P., et al. (2005), Mars surface diversity as revealed by the OMEGA/Mars Express observations, *Science*, *307*, 1576–1581.

Bibring, J.-P., Y. Langevin, J. F. Mustard, F. Poulet, R. Arvidson, A. Gendrin, B. Gondet, N. Mangold, P. Pinet, and F. Forget (2006), Global mineralogical and aqueous Mars history derived from OMEGA/Mars Express data, *Science*, *312*, 400–404.

Bibring, J.-P., et al. (2007), Coupled OMEGA-CRISM Observations of Marwth Vallis, LPSC XXXVIII, abstract #2160, Houston, Tex.

Bishop, J. L. (1996), Visible and infrared reflectance spectroscopy of physical and chemical ferric-smectite mixtures as Mars soil analogs, LPSC XXVII, pp. 117, Houston, Tex.

Bishop, J. L., E. Murad, M. D. Lane, and R. L. Mancinelli (2004), Multiple techniques for mineral identification on Mars: A study of hydrothermal rocks as potential analogues for astrobiology sites on Mars, *Icarus*, *169*(2), 331–323.

Bishop, J. L., et al. (2008a), Phyllosilicate diversity observed by CRISM in Mawrth Vallis: Identification of nontronite, montmorillonite, kaolinite, and hydrated silica, LPSC XXXIX, abstract #2124, Houston, Tex.

Bishop, J. L., et al. (2008b), Phyllosilicate diversity and past aqueous activity revealed at Mawrth Vallis, Mars, *Science*, *321*, 830–833.

Bishop, J. L., M. D. Lane, M. D. Dyar, and A. J. Brown (2008c), Reflectance and Emission Spectroscopy Study of Four Groups of Phyllosilicates: Smectites, Kaolinite-Serpentines, Chlorites and Micas, *Clay Min.*, *43*(1), 35–54.

Bishop, J. L., W. P. Gates, H. D. Makarewicz, N. K. McKeown, and T. Hiroi (2011), Reflectance spectroscopy of beidellites and their importance for Mars, *Clays Clay Min.*, *59*(4), 378–399.

Bishop, J. L., D. Loizeau, N. K. McKeown, L. Saper, M. D. Dyar, D. Des Marais, M. Parente, and S. L. Murchie (2013a), What the ancient phyllosilicates at Mawrth Vallis can tell us about possible habitability on early Mars, *Planet. Space Sci.*, doi:10.1016/j.pss.2013.05.006, in press.

Bishop, J. L., E. B. Rampe, D. L. Bish, L. L. Baker, Z. Abidin, N. Matsue, and T. Henmi (2013b), Spectral and hydration properties of allophane and imogolite, *ClaysClay Min.*, *61*(1), 57–74, doi:10.1346/CCMN.2013.0610105.

Buczkowski, D. L., and K. D. Seelos (2010), Extensive phyllosilicate layer in north-western Noachis Terra: Relationship to phyllosilicates in Holden and Eberswalde? *4th MSL Landing Site Workshop*.

Burns, R. G. (1993), *Mineralogical Applications of Crystal Field Theory*, 551 pp., Cambridge University Press, Cambridge, U.K.

Delamere, W. A., et al. (2010), Color imging of Mars by the High Resolution Imaging Science Experiment (HiRISE), *Icarus*, *205*(1), 38–52.

Edgett, K. S., and M. C. Malin (2000), Examples of martian sandstone: indurated, lithified, and cratered eolian dunes in MGS MOC images, LPSC XXXI, Houston, Tex.

Edgett, K. S., and T. J. Parker (1997), Water on early Mars: Possible subaqueous sedimentary deposits covering ancient cratered terrain in western Arabia and Sinus Meridiani, *Geophys. Res. Lett.*, *24*, 2897–2900.

Farrand, W. H., T. D. Glotch, J. W. Jr.Rice, J. A. Hurowitz, and G. A. Swayze (2009), Discovery of jarosite within the Mawrth Vallis region of Mars: Implications for the geologic history of the region, *Icarus*, *204*(2), 478–488.

Greely, R., and J. E. Guest (1987), Geologic map of the eastern equatorial region of Mars, USGS, Misc. Invest. Series, I-1802-B.

Kindle, E., and L. Cole (1938), Some mud crack experiments, *Geologie der Meere und Binnengewasser*, *2*, 278–283.

Lachenbruch, A. H. (1962), Mechanisms of thermal contraction cracks and ice-wedge polygons in permafrost, *Geol. Soc. Am. Special Papers*, *70*, 1–69.

Le Deit, L., O. Bourgeois, D. Mege, E. Hauber, S. Le Mouelic, M. Masse, R. Jaumann, and J. Bibring (2010), Morphology, stratigraphy, and mineralogical composition of a layered formation covering the plateaus around Valles Marineris, Mars: Implications for its geological history, *Icarus*, *208*, 684–703.

Le Deit, L., J. Flahaut, C. Quantin, E. Hauber, D. Mege, O. Bourgeois, J. Gurgurewicz, M. Masse, and R. Jaumann (2012), Extensive surface pedogenic alteration of the Martian Noachian crust suggested by plateau phyllosilicates around Valles Marineris, *J. Geophys. Res.*, *117*, E00J05, doi:10.1029/2011JE003983.

Levy, J., J. W. Head, III, and D. Marchant (2009), Thermal contraction crack polygons on Mars: Classification, distribution, and climate implications from HiRISE observations, *J. Geophys. Res.*, *114*, E01007, doi:10.1029/2008JE003273.

Loizeau, D., et al. (2007), Phyllosilicates in the Mawrth Vallis region of Mars, *J. Geophys. Res.*, *112*, E08S08, doi:10.1029/2006JE002877.

Loizeau, D., N. Mangold, F. Poulet, V. Ansan, E. Hauber, J. Bibring, B. Gondet, Y. Langevin, P. Masson, and G. Neukum (2010), Stratigraphy in the Mawrth Vallis region through OMEGA, HRSC color imagery and DTM, *Icarus*, *205*(2), 396–418.

Loizeau, D., S. C. Werner, N. Mangold, J.-P. Bibring, and J. L. Vago (2012), Chronology of deposition and alteration in the Mawrth Vallis region, Mars, *Planet. Space Sci.*, *72*, 31–43.

McEwen, A. S., et al. (2007), Mars Reconnaissance Orbiter's High Resolution Imaging Science Experiment (HiRISE), *J. Geophys. Res.*, *112*, E05S02, doi:10.1029/2005JE002605.

McKeown, N. K., J. L. Bishop, E. Z. Noe Dobrea, M. Parente, B. L. Ehlmann, J. F. Mustard, S. L. Murchie, G. A. Swayze, J. Bibring, and E. A. Silver (2009), Characterization of phyllosilicates observed in the central Mawrth Vallis region, Mars, their potential formational processes, and implications for past climate, *J. Geophys. Res.*, *144*, E00D10, doi:10.1029/2008JE003301.

McKeown, N. K., J. L. Bishop, J. J. Wray, E. Z. Noe Dobrea, and E. A. Silver (2010), Textures and morphologies of phyllosilicate-bearing units at Mawrth Vallis, LPSC XL, abstract #2433, Houston, Tex.

McKeown, N. K., J. L. Bishop, J. Cuadros, S. Hillier, E. Amador, H. D. Makarewicz, M. Parente, and E. A. Silver (2011), Interpretation of reflectance spectra of clay mineral-silica mixtures: implications for martian clay mineralogy at Mawrth Vallis, *Clays Clay Min.*, *59*(4), 400–415.

Mellon, M. T. (1997), Small-scale polygonal features on Mars: Seasonal thermal contraction cracks in permafrost, *J. Geophys. Res.*, *102*, 25617–25628.

Mellon, M. T., R. E. Arvidson, J. J. Marlow, R. J. Phillips, and E. Asphaug (2008), Periglacial landforms at the Phoenix landing site and the northern plains of Mars, *J. Geophys. Res.*, *113*, E00A23, doi:10.1029/2007JE003039.

Milliken, R. E., et al. (2008), Opaline Silica in Young Deposits on Mars, *Geology*, *36*(11), 847–850.

Murchie, S., et al. (2007), Compact Reconnaissance Imaging Spectrometer for Mars (CRISM) on Mars Reconnaissance Orbiter (MRO), *J. Geophys. Res.*, *112*, E05S03, doi:10.1029/2006JE002682.

Murchie, S. L., et al. (2009), Compact Reconnaissance Imaging Spectrometer for Mars investigation and data set from the Mars Reconnaissance Orbiter's primary science phase, *J. Geophys. Res.*, *114*, E00D07, doi:10.1029/2009JE003344.

Mustard, J. F., et al. (2008), Hydrated silicate minerals on Mars observed by the Mars Reconnaissance Orbiter CRISM instrument, *Nature*, *454*, 305–309.

Noe Dobrea, E. Z., et al. (2008), Clay bearing units in the region around Mawrth Vallis: stratigraphy, extent, and possible alteration fronts, LPSC XXXIX, abstract #1077, Houston, Tex.

Noe Dobrea, E. Z., et al. (2010), Mineralogy and Stratigraphy of Phyllosilicate-bearing and Dark Mantling Units in the Greater Mawrth Vallis/ West Arabia Terra Area: Constraints on Geological Origin, *J. Geophys. Res.*, *115*, E00D19, doi:10.1029/2009JE003351.

Noe Dobrea, E. Z., J. R. Michalski, and G. A. Swayze (2011), Aqueous mineralogy and stratigraphy at and around the proposed Mawrth Vallis landing site: new insights into the aqueous history of the region, *Mars*, *6*, 32–46.

Parente, M. (2008), A new approach to denoising CRISM images, LPSC *XXXIX*, Houston, Tex.

Pelkey, S. M., et al. (2007), CRISM multispectral summary products: Parameterizing mineral diversity on mars from reflectance, *J. Geophys. Res.*, *112*, E08S14, doi:10.1029/2006JE002831.

Plummer, P. S., and V. A. Gostin (1981), Shrinkage Cracks: Desiccation or Synaeresis?, *J. Sediment. Petrol.*, *51*(4), 1147–1156.

Poulet, F., J.-P. Bibring, J. F. Mustard, A. Gendrin, N. Mangold, Y. Langevin, R. E. Arvidson, B. Gondet, and C. Gomez (2005), Phyllosilicates on Mars and implications for the early Mars history, *Nature*, *438*, 632–627.

Poulet, F., N. Mangold, D. Loizeau, J. Bibring, Y. Langevin, J. R. Michalski, and B. Gondet (2008), Abundance of minerals in the phyllosilicate-rich units on Mars, *Astron. Astrophys.*, *487*, L41–L44.

Scott, D. H., and K. L. Tanaka (1986), Geologic map of western equatorial region of Mars, USGS, Misc. Invest. Series, I-1802-A.

Sullivan, R., R. E. Arvidson, J. P. Grotzinger, A. Knoll, M. P. Golombek, B. Jolliff, S. W. Squyres, and C. Weitz (2007), Aeolian geomorphology with MER Opportunity at Meridiani Planum, Mars, LPSC XXXVIII, Houston, Tex.

Swartz, J. H. (1927), Subaerial sun-cracks, *Am. J. Sci.*, *14*, 69–70.

Wray, J. J., S. W. Squyres, B. L. Ehlmann, J. F. Mustard, and HiRISE Team (2007), Meter-scale morphology and stratigraphy of phyllosilicate-rich outcrops in Mawrth Vallis, *7th Int'l Mars Conf.*, Pasadena, Calif.

Wray, J. J., B. L. Ehlmann, S. W. Squyres, J. F. Mustard, and R. L. Kirk (2008), Compositional stratigraphy of clay-bearing layered deposits at Mawrth Vallis, Mars, *Geophys. Res. Lett.*, *35*, L12202, doi:10.1029/2008GL034385.

Wray, J. J., S. W. Squyres, L. H. Roach, J. L. Bishop, J. F. Mustard, and E. Z. Noe Dobrea (2010), Identification of the Ca-sulfate bassanite in Mawrth Vallis, Mars, *Icarus*, *209*, 416–421.